Cell PRESS
Neuron
Article

# Linking the Computational Structure of Variance Adaptation to Biophysical Mechanisms

Yusuf Ozuysal[1,3] and Stephen A. Baccus[2,*]
[1]Department of Electrical Engineering
[2]Department of Neurobiology, Stanford University School of Medicine
Stanford University, Stanford, CA 94305, USA
[3]Present address: Google, Inc., Mountain View, CA 94043, USA
*Correspondence: baccus@stanford.edu
DOI 10.1016/j.neuron.2011.12.029

## SUMMARY

**In multiple sensory systems, adaptation to the variance of a sensory input changes the sensitivity, kinetics, and average response over timescales ranging from < 100 ms to tens of seconds. Here, we present a simple, biophysically relevant model of retinal contrast adaptation that accurately captures both the membrane potential response and all adaptive properties. The adaptive component of this model is a first-order kinetic process of the type used to describe ion channel gating and synaptic transmission. From the model, we conclude that all adaptive dynamics can be accounted for by depletion of a signaling mechanism, and that variance adaptation can be explained as adaptation to the mean of a rectified signal. The model parameters show strong similarity to known properties of bipolar cell synaptic vesicle pools. Diverse types of adaptive properties that implement theoretical principles of efficient coding can be generated by a single type of molecule or synapse with just a few microscopic states.**

## INTRODUCTION

The range of natural signals exceeds the dynamic range of neurons. As a result, neural circuits adapt so as to more efficiently encode the recent history of inputs. One widespread example of this process occurs in response to a change in the magnitude of fluctuations, or the variance of a sensory input (Laughlin, 1989). Variance adaptation occurs in many sensory systems, including the vertebrate retina and visual cortex, the fly visual system, and the avian auditory forebrain (Fairhall et al., 2001; Nagel and Doupe, 2006; Ohzawa et al., 1985; Shapley and Victor, 1978; Smirnakis et al., 1997).

When the stimulus environment changes from a low to high variance, temporal filtering quickly accelerates, sensitivity decreases, and the average response increases. (Baccus and Meister, 2002; Chander and Chichilnisky, 2001; Kim and Rieke, 2001). When the environment maintains a high variance, slow changes occur over 1–10 s, comprised mostly of a homeostatic decay in the average response that opposes the fast change in baseline. (Baccus and Meister, 2002; Fairhall et al., 2001; Nagel and Doupe, 2006). Upon a decrease in contrast, all these changes reverse direction. The time constants for slow adaptation are asymmetric, with the baseline decaying faster in high contrast than it rises in low contrast. The remarkable similarity of these properties across species and sensory systems indicates a strong commonality in the encoding of signals that vary in amplitude (Baccus, 2006; Baccus and Meister, 2002; Fairhall et al., 2001 ; Nagel and Doupe, 2006).

In the vertebrate retina, although all of these adaptive changes are observed among ganglion cells and some amacrine cells, there is diversity in the adaptive properties of different cell populations. For example, Off cells change their gain more than On cells, and On cells show less of a change in temporal processing (Beaudoin et al., 2008; Chander and Chichilnisky, 2001). Bipolar cells also vary in their adaptive properties, with some cells not adapting, whereas others change only their gain or their temporal processing, or do not exhibit slow changes in baseline (Baccus and Meister, 2002; Rieke, 2001).

There is also diversity in the potential mechanisms that have been proposed for contrast adaptation in retinal ganglion cells (Demb, 2008). Inactivation of voltage-dependent Na channels in ganglion cells can quickly change the gain (Kim and Rieke, 2003). In addition, a large fraction of adaptation occurs as the signal travels through the synapse from bipolar to ganglion cell (Beaudoin et al., 2007; Zaghloul et al., 2005). A change in basal vesicle release is proposed to cause slow contrast adaptation, and another calcium-related mechanism, such as channel inactivation, might cause fast adaptation (Beaudoin et al., 2008; Demb, 2008; Manookin and Demb, 2006).

Across sensory systems, a substantial difficulty in connecting the apparently complex and diverse phenomena of variance adaptation with the set of potential cellular mechanisms is the lack of a quantitative model that captures both the immediate sensory response and all adaptive properties. Although several models have been proposed for contrast adaptation (Gaudry and Reinagel, 2007 ; Mante et al., 2008 ; Shapley and Victor, 1979), they focused on only a few aspects of adaptation or used abstract components that lack a clear connection to biophysical mechanisms. In addition, previous efforts to describe the rules of contrast adaptation using a model were constrained only by the firing rate of spiking neurons and not by the membrane potential response.

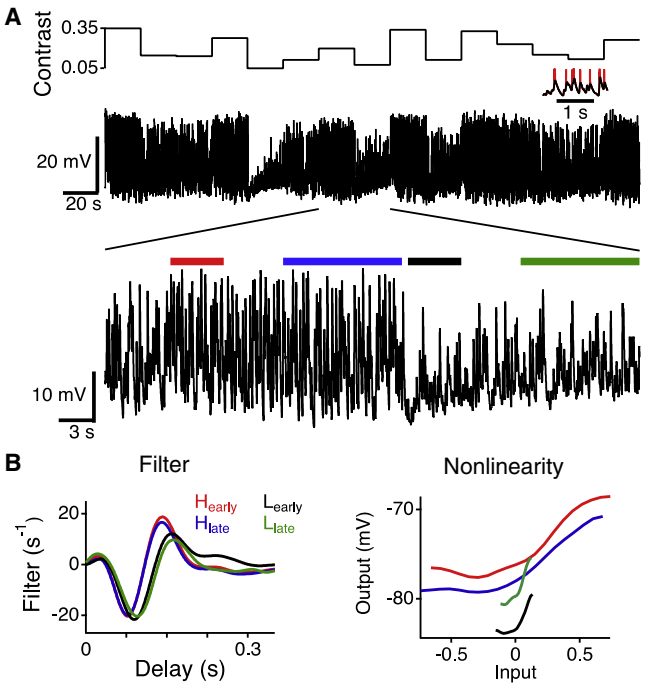


**Figure 1. Ganglion Cell Membrane Potential Response to Changing Contrast**

(A) Top, contrast of a randomly flickering stimulus drawn from a Gaussian intensity distribution with a constant mean. Contrast values of 3%–30% were presented for periods of 20 s. Middle, the membrane potential response of a ganglion cell. The inset shows the recording before and after the spikes were removed. Bottom, expanded segment showing contrast transitions. Colored bars indicate intervals $H_{early}$, 1–5 s after a step to high contrast, $H_{late}$, 15–20 s after a high-contrast step, $L_{early}$ and $L_{late}$, defined as similar time intervals after a low-contrast step.

(B) Linear-nonlinear models of different intervals indicated by the colored bars in (A).

Here, we present a simple theoretical framework that combines aspects of models previously used to capture sensory responses and cellular mechanisms, and use it to interpret the adaptive behavior of retinal neurons. Our goals were to accurately predict the intracellular membrane potential response to a uniform field stimulus with a constant mean intensity across a wide range of contrasts and to capture all adaptive properties with a model that has a natural relationship to biophysical properties. We also wanted the model to be sufficiently simple to allow insight into how its mechanics give rise to the multiple properties of adaptation.

## RESULTS

We presented to the isolated salamander retina a spatially uniform visual stimulus that flickered randomly, and recorded the intracellular membrane potential responses from inner retinal neurons. The intensity changed every 30 ms and was drawn from a Gaussian distribution with a constant mean to avoid contributions from luminance adaptation. Temporal contrast also varied randomly by changing the standard deviation of the distribution every 20 s, with each sequence lasting 300 s and having 15 contrasts (Figure 1A). To isolate the strong component of adaptation that occurs prior to spiking (Baccus and Meister, 2002; Kim and Rieke, 2001; Zaghloul et al., 2005), we digitally removed spikes from the recording to analyze the subthreshold membrane potential.

Adaptive properties of neurons have been quantified using a linear-nonlinear (LN) model (see Experimental Procedures) consisting of a linear temporal filter passed through a static nonlinearity. The linear filter represents the average feature that depolarizes the cell, and the nonlinearity represents the average instantaneous comparison between the filtered visual stimulus and the response. Both quantities are average measures given a particular set of stimulus statistics; the underlying system is more complex with additional nonlinearities (Baccus and Meister, 2002; Kim and Rieke, 2001). Thus, the LN model can reveal and quantify adaptation but does not produce adaptation itself. When LN models are used to represent different time intervals relative to a contrast step, the most accurate linear filter changes, as does the nonlinearity, indicating the presence of an adaptive response (Figure 1B). A high contrast step quickly accelerates temporal processing, as measured by the time to peak of the linear filter, makes the temporal response more differentiating, and decreases the sensitivity, which is defined as the average slope of the nonlinearity (Demb, 2008). High contrast also quickly produces a depolarizing offset, as measured by the average value of the nonlinearity, that then slowly decays. We then tested a new model to capture both the intracellular membrane potential (Figure 1A) and adaptive properties (Figure 1B) across multiple contrasts.

### The Linear-Nonlinear-Kinetic Model

Many biophysical mechanisms produce changes in gain, including ion channel inactivation, biochemical cascades, receptor desensitization, and synaptic depression (Burrone and Lagnado, 2000; DeVries and Schwartz, 1999; He et al., 2002). A widely used approach to describe these mechanisms uses a first-order kinetic model, whereby a system transitions between different states and is governed by a set of rate constants (Colquhoun and Hawkes, 1977; Hodgkin and Huxley, 1952). Initially, we sought to capture adaptive properties with a kinetic model, without regard to any one corresponding mechanism. A simple example of such a model has four states (Figure 2A). The first state represents a pool of available molecules or signaling elements in a resting state ($R$), such as closed ion channels or receptors, synaptic vesicles in the readily releasable pool (RRP), or an inactive enzyme in a biochemical cascade. The second state is the active state ($A$), which is the output of the system. This state would represent open ion channels, activated receptors, or an active enzyme or neurotransmitter in the synaptic cleft released from vesicles. The third and fourth states, $I_1$ and $I_2$, represent inactivated states, such as inactivated ion channels, desensitized receptors, or depleted pools of synaptic vesicles. Each signaling element can occupy one of the states, and the rate of transition between the states is governed by a set of first-order differential equations (see Experimental Procedures). Rate constants are either fixed or vary in time by being scaled multiplicatively by an input. The coupling of an input

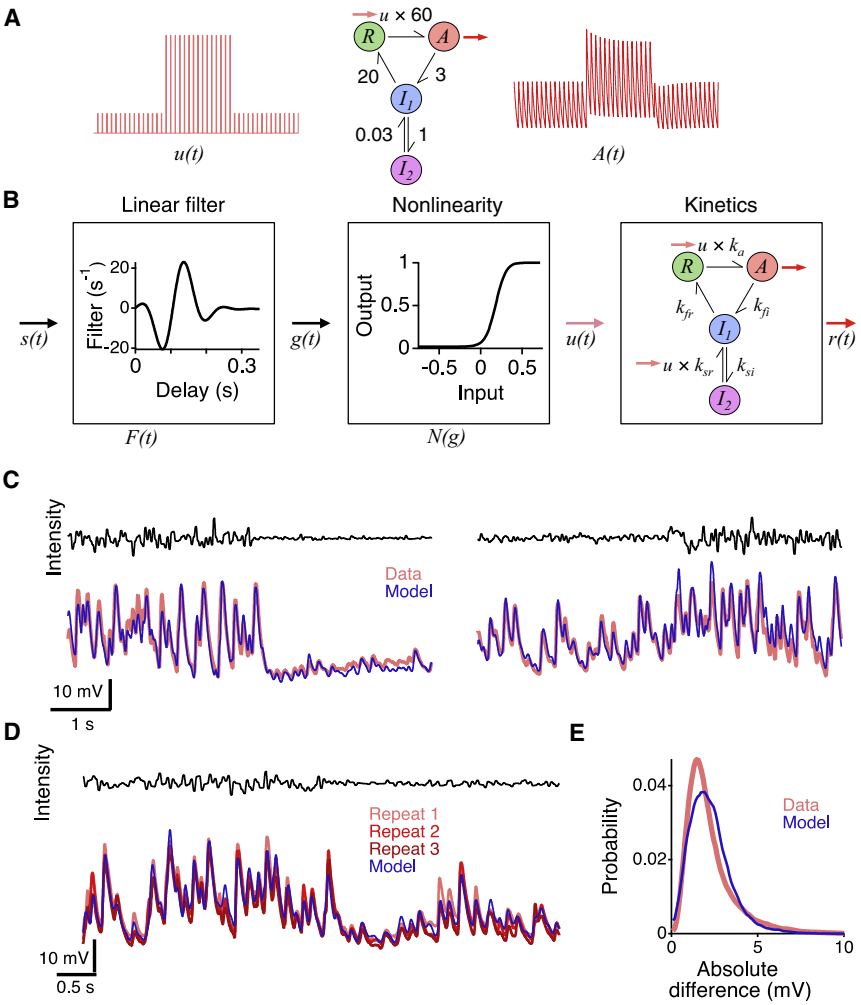


**Figure 2. The LNK Model**

(A) A train of impulses that changed from low- to high-amplitude is shown as an input, $u(t)$, presented to a first-order kinetic model with four states. Numbers indicate rate constants for transitions between the resting ($R$), active ($A$), and inactivated states, ($I_1$ and $I_2$). The rate constant between resting and active states is modulated by $u(t)$. The output is the occupancy of the active state ($A(t)$).

(B) The LNK model. The input, $s(t)$, is convolved with a linear temporal filter, $F_{LNK}(t)$, and then passed through a static nonlinearity, $N_{LNK}(g)$, that does not change with contrast. The output of the nonlinearity, $u(t)$, controls two rate constants in the kinetics block, one that leads to the active state and one that accelerates recovery from the inactivated state, $I_2$. Other rate constants are fixed, and the output of the model $r'(t)$ is the active state.

(C) The membrane potential of an adapting amacrine cell compared to the LNK model output for a transition to low contrast (left) and to high contrast (right).

(D) The LNK model compared to the amacrine cell response for three repeats of an identical stimulus sequence.

(E) The distribution of the absolute difference in membrane potential between responses to an identical stimulus compared to the distribution of the difference between the model output and membrane potential responses. Results are combined for six cells with three repeated responses across the entire recording.

to the system is analogous to a reaction rate that depends on the concentration of the reactants. For example, the change in the active state is described by

$$\frac{dA}{dt} = \text{inflow} - \text{outflow} = k_a u(t) R(t) - k_{fi} A(t), \qquad \text{(Equation 1)}$$

where $R(t)$ and $A(t)$ are the occupancies of the resting and active states, $k_a$ and $k_{fi}$ are constants, and $u(t)$ is the input that scales the activation rate constant, $k_a$.

When a train of pulses of either small or large amplitude drives the four-state system, the larger input produces output pulses with a smaller gain and also increases the baseline (Figure 2A). To produce dynamics with both fast and slow timescales, the fourth state ($I_2$) couples to the first inactivated state ($I_1$), using slower rate constants. As a result, a slow shift in baseline occurs following a change in the amplitude of the input. The rate constants in the four-state model are the rates of activation ($k_a$), fast inactivation ($k_{fi}$), fast recovery ($k_{fr}$), slow inactivation ($k_{si}$), and slow recovery ($k_{sr}$).

Although this four-state system can produce adaptive changes, it lacks the temporal filtering and selectivity of retinal neurons. At a fixed mean luminance, photoreceptors are nearly linear. Strong rectification first appears in amacrine and ganglion cells, coinciding with strong contrast adaptation (Baccus and Meister, 2002; Kim and Rieke, 2001; Rieke, 2001). This threshold likely arises from voltage-dependent calcium channels in the bipolar cell synaptic terminal (Heidelberger and Matthews, 1992), a point that would occur prior to adaptive changes in sensitivity in the presynaptic terminal or postsynaptic membrane. Thus, we combined the adaptive system with a linear-nonlinear model, yielding a system with a linear temporal filter, a static nonlinearity, and an adaptive kinetics block (Figure 2B). In this linear-nonlinear-kinetic (LNK) model, the kinetics block contributes both to the overall temporal filtering and the sensitivity of the system, making these properties depend on the input. Thus, the linear filter ($F_{LNK}$) and nonlinearity ($N_{LNK}$) of the LNK model are not the same as the filter and nonlinearity, $F_{LN}$ and $N_{LN}$, respectively, in an LN model fit to the entire response. To couple the initial linear-nonlinear system to the kinetics block, the output of the nonlinearity, $u(t)$, scales one or two rate constants. Although this means that the transition rate is proportional to the nonlinearity output, a higher-order dependence—such as the dependence of vesicle release on a higher power of the calcium concentration—can be captured in the nonlinearity itself.

We fit LNK models using a constrained optimization algorithm (see Experimental Procedures). The filter and nonlinearity were

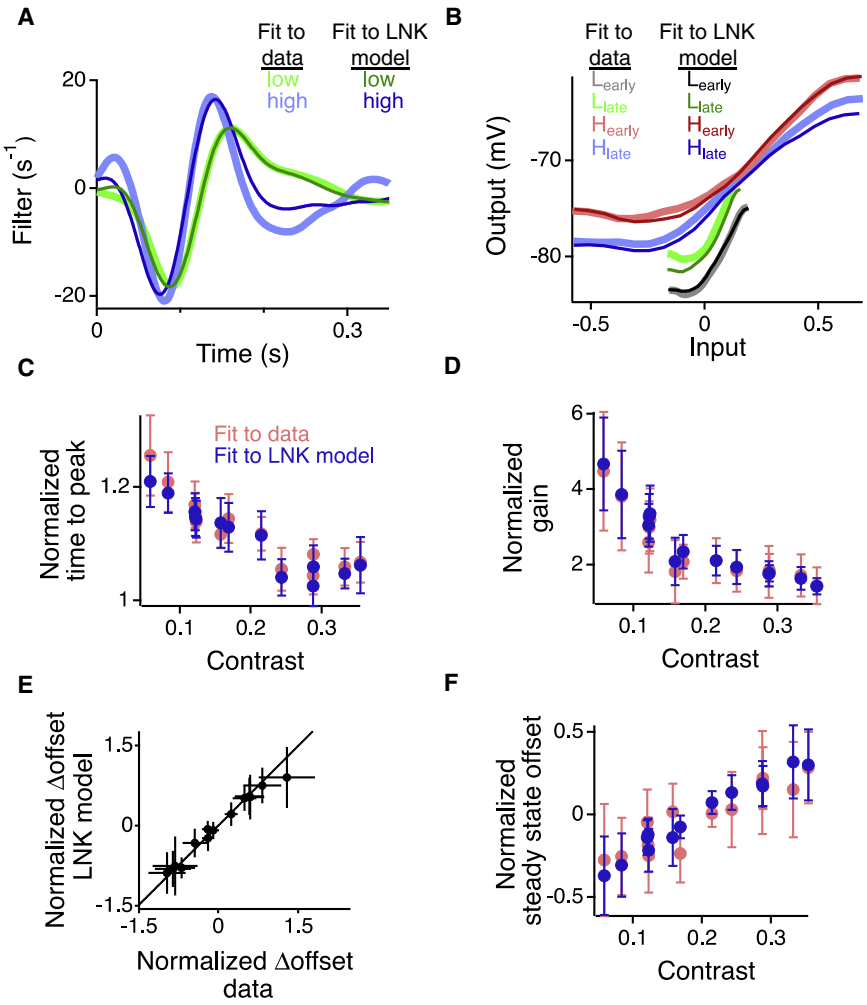


**Figure 3. The LNK Model Captures Retinal Contrast Adaptation**

(A and B) Linear-nonlinear models were computed for the membrane potential response of a ganglion cell during $H_{early}$, $H_{late}$, $L_{early}$ and $L_{late}$. LN models were also fit to the output of an LNK model. Left, linear filters, $F_{LN}(t)$, for all low (8%) or high contrast (35%), fit to the recording and LNK model. Right, static nonlinearity, $N_{LN}(g)$, for all four intervals fit to the recording and LNK model.

(C) The change in the peak of the linear temporal filter, $F_{LN}$, of an LN model fit to the membrane potential or to the LNK model. Results for (C–F) are averaged across 12 amacrine and ganglion cells.

(D) Average sensitivity computed as the average slope of the nonlinearity, $N_{LN}$, of an LN model fit to the response or to the LNK model as a function of contrast.

(E) The normalized change in average membrane potential after a contrast switch, compared between a cell's response and its LNK model. Normalization was performed by subtracting the mean and dividing by the standard deviation of the entire recording.

(F) The normalized average membrane potential at the end of a contrast period for each cell's response and its LNK model as a function of contrast. Error bars indicate standard error.

reduced to a set of 20 parameters, and the kinetics block contributed 5 parameters. The activation rate $k_a$ was scaled by the input, and most other rate constants were fixed. In addition, to capture the contrast dependence of the rate of slow adaptation, the input scaled the rate of slow recovery $k_{sr}$. The motivation for scaling of the slow rate constant by the input is discussed further below.

## Accuracy of the LNK Model

We compared the LNK model output to the cell's membrane potential response across the entire recording (300 s). The model accurately captured the response at all times, including contrast transitions at both decreases and increases in contrast (Figure 2C, Figure S1). The correlation coefficient between the model and the response was 88 ± 4% (90 ± 2% for bipolar cells [n = 5], 89 ± 4% for amacrine cells [n = 9], and 86 ± 4% for ganglion cells [n = 7]), mean ± SEM. We then compared these values to the intrinsic variability of each cell by repeating a stimulus sequence two to three times. The accuracy of the model was nearly that of the variability between repeats of the stimulus, which was 90 ± 5% (92 ±2% for bipolar cells, 92 ± 4% for amacrine cells, and 89 ± 6% for ganglion cells) (Figures 2D and 2E). Thus, the LNK model accurately captured the membrane potential response to changing contrast for inner retinal neurons.

## The LNK Model Captures Adaptation

We then assessed how well the LNK model captured adaptive properties by fitting LN models to both the data and to the LNK model. Examining the temporal filters of these LN models, the LNK model captured the fast change in temporal processing between low and high contrast (Figure 3A). In addition, the LNK model captured fast changes in sensitivity between low and high contrast as well as fast and slow changes in baseline membrane potential (Figure 3B). Across a population of cells, the LNK model closely matched the temporal filtering and average overall sensitivity of the cell's response across the full range of contrasts (Figures 3C and 3D). After a contrast step, the LNK model matched the fast change in average membrane potential of a cell across a range of contrast transitions (Figure 3E). Finally, the LNK model matched slow changes in baseline as the model matched the near steady-state average membrane potential value of a cell at the end of 20 s of constant contrast (Figure 3F). Thus, the LNK model accurately captured both the membrane potential response and all adaptive properties of inner retinal neurons.

## How an LNK System Adapts to the Variance

Figure 4 illustrates how the dynamics of the LNK model generate variance adaptation. The initial linear filter selects a particular feature of the stimulus. Then, the nonlinearity rectifies the signal,

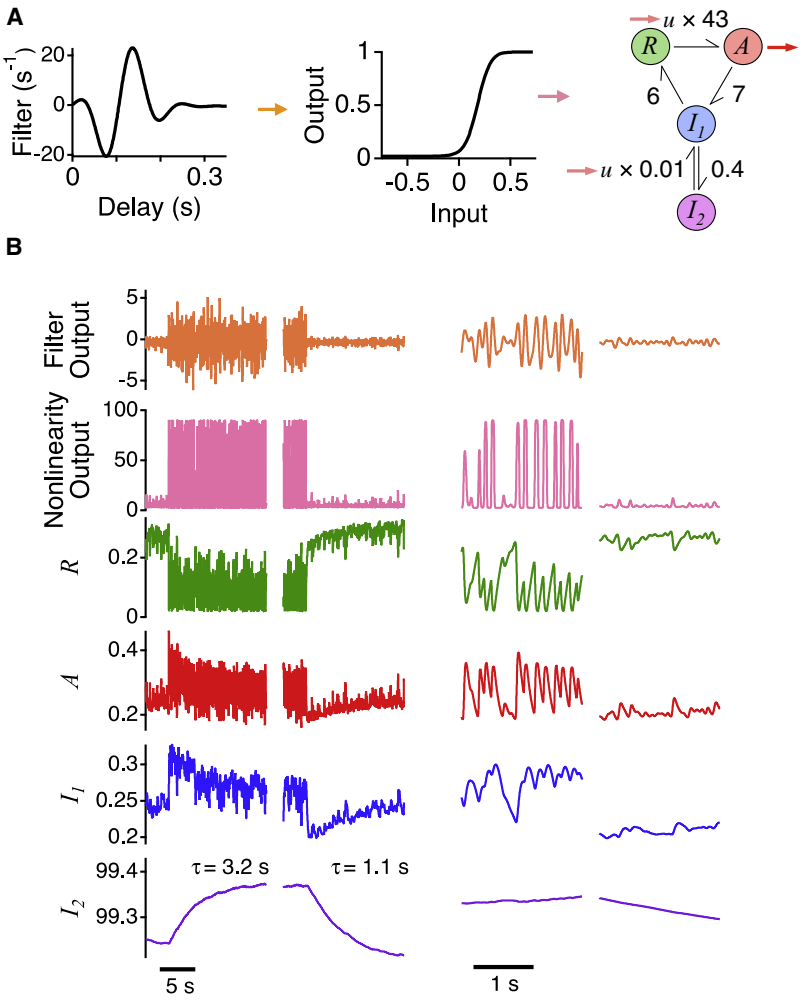


**Figure 4. Internal Dynamics of the LNK Model**

(A) LNK model of an adapting ganglion cell. Colored arrows and states indicate the output of different stages and state occupancies shown in (B).

(B) Top to bottom, the output of the linear filter, the output of the nonlinearity, and the state occupancies for each of the four states. Left to right, a transition to high contrast, a transition to low contrast, and segments of high and low contrast at an expanded timescale.

such that when the contrast changes, the output of the nonlinearity changes not only its standard deviation but also its mean and other statistics. Adaptation is then accomplished by the action of the kinetic model.

When the contrast increases, the input to the kinetics block increases its mean value, thus increasing the activation rate constant. As a result, the increase in contrast automatically accelerates the response. The resulting increase in the occupancy of the active state depletes the resting state. We define the gain of the kinetics block as the change in the occupancy of the active state, $\Delta A$, caused by a small change in the input, $\Delta u$. In Supplemental Information, we derive that $\Delta A$ is simply a product of the input, $\Delta u$, scaled by the rate constant, $k_a$, and the resting state occupancy, $R$,

$$\frac{\Delta A_{\Delta u}}{\Delta u} = k_a R(t) \Delta t. \qquad \text{(Equation 2)}$$

Thus, the instantaneous gain of the kinetics block is proportional to the resting state occupancy. As such, depletion of the resting state decreases the gain (Figure 4B). As the resting state, $R$, depletes, the inactivated states increase in occupancy at different rates. These inactivated states act as a buffer, controlling the occupancy in the resting and active states. In particular, the slow inactivated state, $I_2$, increases gradually, producing the slow decay in offset seen in the active state. At the transition to low contrast, occupancy of $I_2$ slowly decreases as the resting state recovers.

A key function of the first inactivated state, $I_1$, was revealed by attempting to fit models using other network topologies. We found that when slow rate constants existed on the return path from the active back to the resting state, the fast and slow kinetics became coupled and it was not possible to accurately produce dynamics with both time scales (Figure S2). Thus, state $I_1$ served to generate distinct fast and slow properties. As previously observed, changes in temporal processing occurred quickly, most changes in gain occurred at a fast timescale, and changes in offset occurred with both fast and slow timescales (Baccus and Meister, 2002). At a fine timescale (Figure 4B, right), membrane potential responses are asymmetric, having a faster rise rate than decay. The LNK model generates these responses by first producing brief transients as the output of the nonlinearity. These transients are then filtered by a combination of exponentials produced by the kinetics block (see Figure 7), yielding an asymmetric response.

Fast and slow offsets opposed each other, such that slow offsets produced a homeostatic regulation of the membrane potential (Baccus and Meister, 2002). This effect can be understood as an action of fast and slow subsystems in the kinetics block. At the transition to high contrast, the increase in the average activation rate constant leads to a fast equilibration among the first three states. This increases the mean occupancy of both the active and inactivated state $I_1$ occupancy in the resting state. The increase in the occupancy of $I_1$, however, then leads to a slow equilibration involving the second inactivated state, as $I_2$ slowly steals occupancy from the other states. Thus, the architecture of a fast subsystem linked to a slower reservoir leads to the transient offset, which is then corrected homeostatically toward an intermediate steady-state value.

Slow adaptation is temporally asymmetric, such that adaptation to a contrast increase proceeds faster than to a contrast decrease. This property is consistent with known principles of statistical estimation, such that it takes longer to accurately

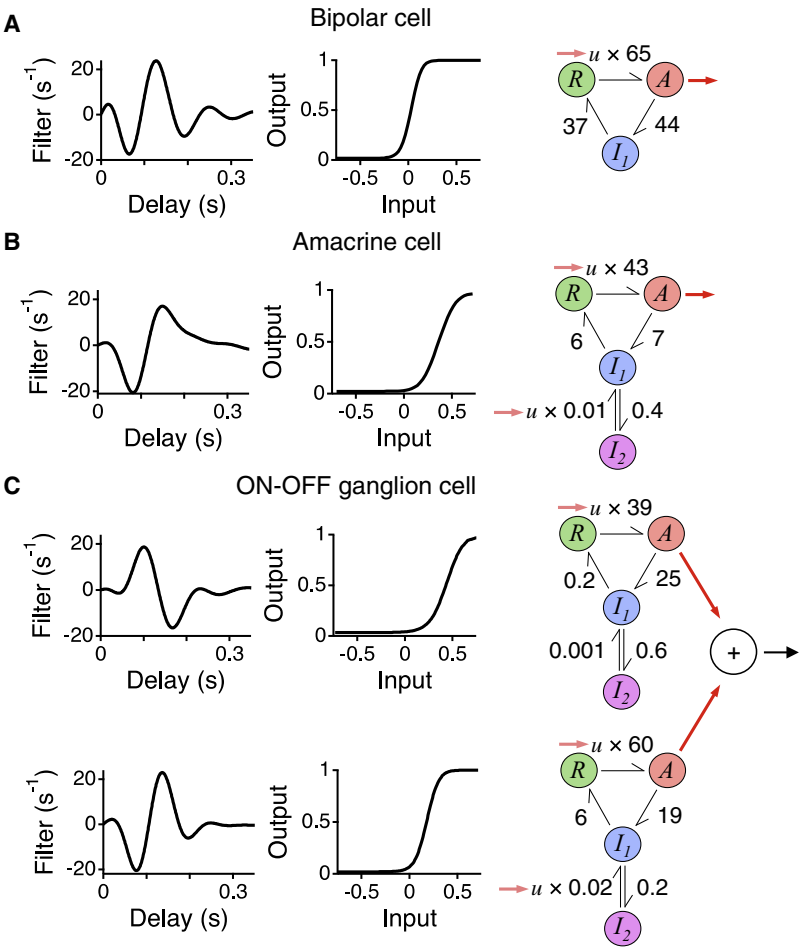


D

Kinetic rate constants

| | $k_a$ | $k_{fi}$ | $k_{fr}$ | $k_{si}$ | $k_{sr}$ |
|---|---|---|---|---|---|
| Bipolar | 23 ± 9 | 50 ± 5 | 87 ± 11 | - | - |
| Amacrine OFF | 95 ± 12 | 8 ± 2 | 5 ± 1 | 1.0 ± 0.5 | 0.03 ± 0.02 |
| Ganglion OFF | 131 ± 20 | 15 ± 8 | 48 ± 20 | 6 ± 3 | 0.02 ± 0.02 |
| Amacrine-Ganglion ON | 39 ± 7 | 45 ± 6 | 1.4 ± 1.8 | 0.30 ± 0.05 | 0.0018 ± 0.001 |

**Figure 5. LNK Models of Different Retinal Neurons**

(A) LNK model of an Off bipolar cell with three kinetic states.

(B) LNK model of an Off transient amacrine cell.

(C) Two-pathway LNK model of an On-Off ganglion cell fit together in a single model. The outputs of the two pathways are summed. For this cell, the relative weighting of the Off pathway was 8.5 times that of the On pathway.

(D) Rate constants for the kinetics block for different cell types and pathways. Shown are averages for 5 Off bipolar cells, 7 Off pathways from Off or On-Off amacrine cells, 5 Off pathways from Off or On-Off ganglion cells, and 12 On pathways from On-Off amacrine or ganglion cells.

estimate the variance of a distribution when the variance decreases (DeWeese and Zador, 1998). However, this asymmetry did not arise with fixed slow rate constants of inactivation, $k_{si}$, and recovery, $k_{sr}$. To achieve this property, it was necessary to scale the rate constant $k_{sr}$ that controlled the transition between $I_2$ and $I_1$ by the nonlinearity output $u(t)$, such that different contrasts produced slow adaptation with different time constants.

An additional aspect revealed by the model is the average occupancy of each of the states, which is controlled by the rate constants. At all times, ~99% of the total occupancy was in the inactivated state, $I_2$. Thus, a small fractional change in $I_2$ results in a larger change in the resting and active states. Biophysically, if a signal is carried by a molecule or synaptic vesicle, a very large part of the system is unavailable to transmit the signal.

## Adaptation in Different Cell Types

Many bipolar cells adapt to contrast but show smaller changes in response properties than amacrine or ganglion cells (Baccus and Meister, 2002; Rieke, 2001). The bipolar response appeared saturated because negative deflections were larger than positive deflections (Figure S3A). This corresponds to saturation in the nonlinearity of an overall LN model $N_{LN}$, as has been observed previously (Baccus and Meister, 2002; Rieke, 2001). However, examining the LNK model for an adapting bipolar cell (Figure 5A), we found that the nonlinearity, $N_{LNK}$, was placed symmetrically around the mean of the output, and did not, in fact, rectify the signal. Instead, this saturation can be explained by the kinetics block producing fast adaptation such that, upon a positive deflection, the gain of the kinetics block quickly drops (Figure S3A). Thus, although the saturating response of the cell at high contrast appears to be caused by an instantaneous nonlinear process, it is in fact due to a fast, time-dependent nonlinearity that can be resolved by the parameters of the adaptive kinetics block.

Compared with bipolar cells, transient amacrine cell responses are more rectified and show greater adaptation (Baccus and Meister, 2002). In the LNK model, the midpoint of the bipolar cell nonlinearity ($N_{LNK}$) was at 7 ± 5% (n = 5) of the input range below the mean. For amacrine and ganglion cells, however, the nonlinearity midpoint was 26 ± 2% (n = 12) above the mean input, thus indicating greater rectification than in bipolar cells (Figures 5B and 5C). In the kinetics block, the path of recovery from the active state back to the resting state ($A$ to $I_1$ to $R$) was slower than that of bipolar cells, such that the slowest rate constant was 43.0 ± 1.8 (n = 5) for bipolar cells but 5.0 ± 0.7 (n = 12) for amacrine and ganglion cells. Finally, amacrine and ganglion cells required a second inactive state $I_2$ linked by slow rate constants.

On-Off ganglion cells were fit using a two-pathway LNK model (Figure 5C). The Off pathway was similar to that of adapting Off

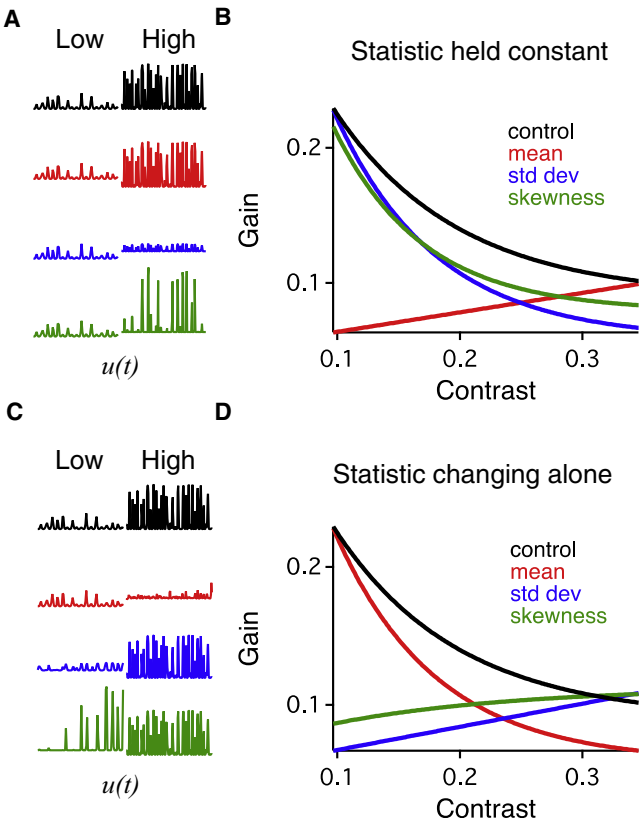


**Figure 6. Variance Adaptation Is Adaptation to the Mean of a Rectified Signal**

(A) Top, the nonlinearity output, $u(t)$, at low and high contrast. Rows 2–4, $u(t)$ with the mean, standard deviation, or skewness held constant, and with other statistics varied as in the control case.

(B) Gain as a function of contrast with the different statistics held constant. Gain was measured as the average occupancy of the resting state, $R(t)$ (Equation 2).

(C) Top, the control nonlinearity output, $u(t)$, at low and high contrast. Rows 2–4, $u(t)$ with the mean, standard deviation, or skewness varying as in the control case, and with the other statistics held constant.

(D) Gain as a function of contrast with the different statistics changing alone.

amacrine cells in its threshold and kinetic parameters. Compared with the Off pathway, the On pathway had a slower filter (as expected), a higher threshold, and different kinetics. The two pathways with separate initial stimulus features and independent adaptive properties likely contribute to the multidimensional stimulus sensitivity observable in retinal ganglion cells (Fairhall et al., 2006).

The different cell types and the On and Off pathways had distinct kinetic parameters (Figure 5D). The precision of these parameter estimates was generally to within 30% (Figure S3B). We examine below how these different parameters give rise to different adaptive behavior.

## Adaptation Is Controlled by the Mean of a Rectified Signal

Because all adaptive properties were localized to the kinetics block, we examined the model to determine which statistics of the internal stimulus representation caused adaptation in the kinetics block. Previous results suggest a correspondence between threshold and adaptation because sustained amacrine cells, which are more linear, also show much less adaptation than transient amacrine cells and ganglion cells (Baccus and Meister, 2002). Because the threshold nonlinearity changes the statistics of the input, we altered the direct input to the kinetics blocks by taking the nonlinearity output and changing its mean, standard deviation, or skewness. To assess adaptation in each case, we measured the average gain of the kinetics block as the average occupancy of the resting state (see Equation 2).

We first kept constant either the mean, standard deviation, or skewness while allowing the other statistics to vary with contrast, as in the control condition. Even though the standard deviation or skewness were kept constant, gain changes were at least as large as occurred in the control condition (Figures 6A and 6B). However, when we kept the mean input constant and varied other statistics, adaptive changes in gain were abolished.

Next, we changed the mean, standard deviation, or skewness and kept the other statistics constant across contrast. In this case, we found that changing the standard deviation or skewness did not cause adaptation and, in fact, produced the opposite effect, causing the gain to increase with increasing standard deviation (Figures 6C and 6D). However, allowing the mean alone to vary caused changes in gain even larger than those that occurred in the control condition.

These results show that changes in the mean input to the kinetics block are both necessary and sufficient to produce adaptation. Thus, in generating adaptation, a key function of the nonlinearity is to transform a change in stimulus contrast into a change in the mean value of the signal. Adaptation to variance can be explained by adaptation to the mean value of a rectified signal.

Thus, from analysis of the model, we propose that bipolar cells and sustained amacrine and ganglion cells, all of which have less of a threshold in their response, experience less adaptation because the output of this threshold changes its mean value less in response to a change in contrast. In comparison, transient amacrine and ganglion cells with a sharp threshold (Figures 5B and 5C) experience greater changes in the mean value of the input to the kinetics block.

## Instantaneous Change in Kinetics, Delayed Change in Gain

Fast adaptation consists of nonlinear response properties that unfold on a timescale similar to the integration time of the response. To measure fast adaptation, previous studies used LN models computed in small time intervals to assess how adaptation changed the response near a contrast transition (Baccus and Meister, 2002). This approach, however, has limited temporal resolution due to the amount of data that can be collected in such small intervals.

In the LNK model, because all adaptive properties are localized to the kinetics block, we assessed how signal transmission of this stage changed at different times during the contrast transition. Because adaptation of the kinetics block is controlled by the mean of the input $u(t)$, we simulated a contrast transition by producing a step change in $u(t)$. Then, we assessed the impulse response of the kinetics block alone by adding a small

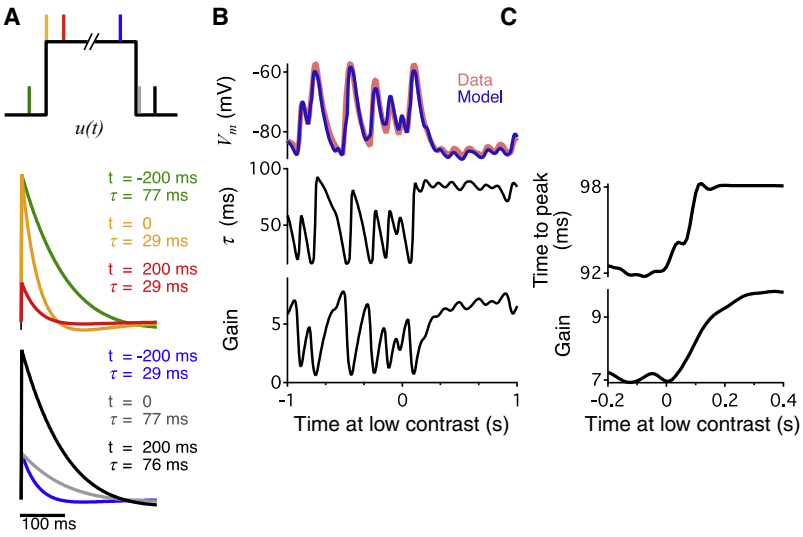


**Figure 7. Change in Kinetics Precedes the Change in Gain**

(A) Top, input to the kinetics block, $u(t)$, consisting of brief impulses, $\Delta u$, added at different times relative to a change in the baseline value of $u(t)$. Middle, impulse response, $F_k(t)$, of the kinetics block resulting from $\Delta u$ at different times relative to an increase in $u(t)$. Bottom, $F_k(t)$ at different times relative to decrease in $u(t)$.

(B) Top, membrane potential and LNK model of an amacrine cell at a transition from 35% to 5% contrast. Impulses $\Delta u$ were added to the kinetics block input $u(t)$ at different times, separated by 10 ms relative to the contrast transition. Middle, time constant of $F_k(t)$ at different times relative to the change in contrast. This time constant was measured as a single exponential fit to $F_k(t)$. Bottom, gain measured as the amplitude of $F_k(t)$ at different times relative to the change in contrast.

(C) For the contrast transition shown in (B), small impulses, $\Delta s$, were added to the stimulus, $s(t)$, and presented to the LNK model at different times, separated by 10 ms relative to the contrast transition. The resulting change in the model output, $r'(t)$, averaged over many stimulus sequences of $s(t)$, was taken as the impulse response to $\Delta s$. Top, the time to peak of the impulse response to $\Delta s$. Bottom, amplitude (rms) of the impulse response to $\Delta s$.

incremental impulse $\Delta u$ at different times relative to the step transition. We measured the change in the active state $A_\Delta(t)$ resulting from the added impulse. This change was a decaying exponential whose amplitude and time constant depended on the time relative to the contrast transition (Figure 7A). We found that the average temporal filtering of the kinetics block to an incremental input changed instantaneously at the increase in mean input, whereas the gain lagged several hundred ms.

We then measured changes in the impulse response of the kinetics block generated by visual input that was presented to the beginning of the model. We chose a segment of data near a contrast transition accurately fit by the model (Figure 7B) and measured the impulse response near the contrast transition by presenting a small $\Delta u$ to the kinetics block at different time points. We then measured the time constant and gain from the resulting change, $A_\Delta(t)$, in the active state. From the model, we found that both the time constant and the instantaneous gain fluctuated quickly in the high contrast environment. Thus, even at a fixed contrast, the gain and temporal filtering change continually depending on the recent input sequence. Although an LN model is a reasonable approximation to inner retinal neurons at a fixed contrast (Chichilnisky, 2001), the LN model fails to capture this ongoing adaptation of the response (Figure S4).

Because the LNK model accurately captures the response during a contrast transition, we assessed how the overall system changed its gain and temporal processing at a fine time resolution. We presented to the first stage of a LNK model small impulses, $\Delta s$, added to different sequences of a white noise input at all 10 ms intervals relative to a decrease in contrast, and then measured the resulting incremental response in the active state. We found that the time to peak of the resulting response changed within the integration time of the filter but that the gain lagged up to twice the integration time of the filter (Figure 7C).

Effects at a contrast transition can be understood in terms of the dynamics of the kinetics block. When the contrast changes, rate constants change as soon as the input to the kinetics block increases. This is because the overall temporal filtering of the kinetics block is set by the eigenvalues of the system (Luenberger, 1979), which are, in turn, a function of the instantaneous rate constants. Because of the causal relationship between the rate constants and the state occupancies, after the rate constants change the resting state occupancy then shifts, thereby changing the gain and the baseline membrane potential. Thus, in an adaptive system of the type represented in the kinetics block, the secondary changes of gain and baseline response necessarily lag the change in the speed of the response, which limits how fast the system can control its gain in response to changing signal amplitude.

## Different Parameters Generate Different Behaviors

To understand how the different parameters of the LNK model generated different adaptive behavior, we first examined differences between Off and On cells. Both cell types change their gain, but On cells have less of a change in temporal filtering (Beaudoin et al., 2008). Compared to the Off cell LNK model, the On cell had a slower filter, a higher threshold in its nonlinearity, and a different set of rate constants (Figure 5C). To test whether differences in rate constants yielded the different adaptive behavior, we measured the impulse response function of the kinetics block alone.

Because contrast adaptation in the LNK model can be explained by adaptation in the kinetics block to the mean value of the input (Figure 6), we represented high and low contrast by two different mean values and then presented impulses riding on the two different baselines. We found that the impulse response of the kinetics block also showed differences between On and Off cells, with On cells showing little change in temporal filtering (Figure 8A and 8B). Compared to the Off pathway, the

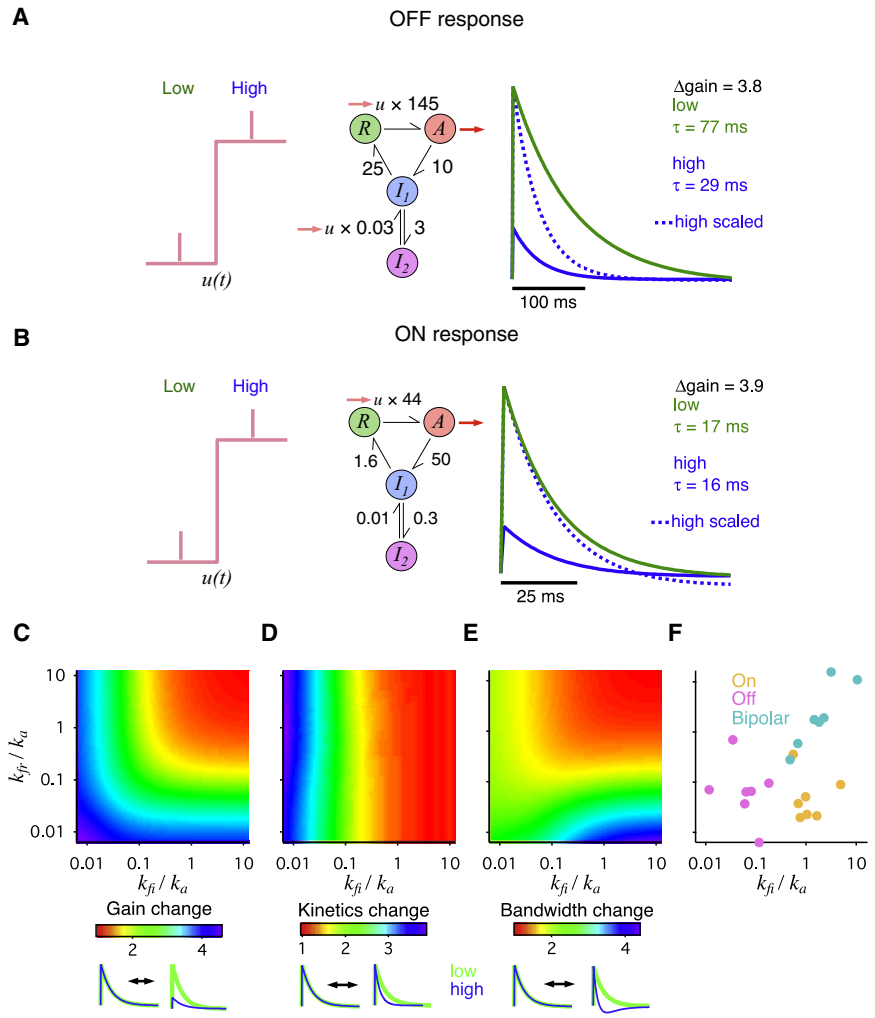


**Figure 8. Different Kinetic Parameters Give Rise to Different Adaptation Properties**

(A) Left, input to the kinetics block used to measure $F_k$, consisting of impulses, $\Delta u$, added to a constant baseline input, $u(t)$. Middle, a four-state kinetics block from the Off pathway. Right, $F_k$ at low and high contrast, and the high contrast $F_k$ rescaled in amplitude.

(B) Same as (A) for a ganglion cell On pathway.

(C) The change in gain of the kinetics block in panel (A) between low and high contrast as a function of two parameters, fast inactivation ($k_{fi}$) and fast recovery ($k_{fr}$). Both parameters were normalized by the mean activation rate ($k_a$).

(D) The change in the time constant of $F_k$ at low and high contrast as a function of $k_{fi}/k_a$ and $k_{fr}/k_a$.

(E) The change in shape of $F_k$ as a function of $k_{fi}/k_a$and $k_{fr}/k_a$, computed as the area of positive values of $F_k$ divided by the total area between the curve and zero.

(F) Different parameter values of $k_{fi}/k_a$ and $k_{fr}/k_a$ for different cell types.

model of the On pathway showed differences in the rates of fast inactivation, $k_{fi}$, and fast recovery from inactivation, $k_{fr}$ (Figure 5D).

We further explored the space of these two parameters ($k_{fi}$ and $k_{fr}$) by measuring the impulse response at different contrasts for many different parameter values, thereby mapping the effects of $k_{fi}$ and $k_{fr}$ on changes in gain, temporal response, and the biphasic temporal response. Changes in gain resulted when either fast inactivation or recovery were slow compared to activation, thus leading to depletion of the resting state during increased activation (Figure 8C). Considering a simplified three-state system at equilibrium, the inflow and outflow of all states are the same (i.e., $R_\infty u_\infty k_a = A_\infty k_i = I_\infty k_r$), where $u_\infty$ is a steady input to the kinetics block. The equilibrium occupancy of the resting state can then be solved as

$$R_\infty = (1 + u_\infty c_1)^{-1}, \qquad \text{(Equation 3)}$$

where $c_1 = (k_a/k_i + k_a/k_r)$. Thus, when either $k_i$ or $k_r$ are small compared to $k_a$, $c_1$ becomes large and weights the effect of the input $u_\infty$ more heavily. This changes the resting state occupancy and, therefore, the gain (see Equation 2) significantly with contrast. This relationship allows the adaptive change in gain to be approximated analytically directly from the rate constants of the model (Figure S5A).

Contrast-dependent changes in temporal filtering occurred when fast inactivation ($k_{fi}$) was prolonged but such changes were unaffected by the rate constant of fast recovery ($k_{fr}$) (Figure 8D). Because of the lack of dependence on $k_{fr}$, we considered a simplified system of three states with no return pathway, $R \xrightarrow{uk_a} A \xrightarrow{k_{fi}} I$. We can derive that the impulse response of this system is a weighted sum of two exponentials (see Supplemental Experimental Procedures), one with a time constant, $u_\infty(\sigma)k_a$, that depends on the contrast ($\sigma$), and one with time constant, $k_{fi}$, that is independent of contrast. The weighting between these two exponentials is set by a constant that depends on the contrast and the inactivation rate such that when $k_{fi}/k_a$ is small, the variable exponential is weighted more heavily. We can use this understanding to predict the adaptive change in temporal filtering directly from the rate constants of the model (Figure S5B).

Finally, the change in differentiation of the temporal filter was produced primarily by fast recovery, with some dependence on fast inactivation as well (Figure 8E). By comparing the state occupancies to the impulse response, $F_k$, we saw that $F_k$ was more biphasic when the increase in the inactivated state $I_1$ exceeded the depletion of the resting state (Figure S5C). Consequently, when recovery was slow, as compared to the steps of activation and inactivation, there was transiently a higher level of inactivation, causing an undershoot in the level of activation. Thus, the three rate constants give flexibility to a system to control its gain and temporal filtering as a function of contrast, although not every behavior is possible with this type of simple system.

We then examined the actual model parameters of different cell types and found that different cells occupied different regions of this parameter space, such that On and Off pathways were distinct from each other and also from bipolar cells (Figure 8F). Bipolar cells, having a faster $k_{fi}$ and $k_{fr}$, showed smaller changes in gain and temporal filtering. Off cells with a slower $k_{fi}$ showed greater gain changes and changes in the time to peak of their overall temporal filter. On cells with a faster $k_{fi}$ but slower $k_{fr}$ showed a substantial gain change and less change in the speed of the temporal filter but a substantial change in the temporal differentiation of the filter. By choosing different rates of inactivation and recovery, simple kinetic systems can produce different adaptive behavior.

### Correspondence of Kinetic Properties with Those of Synaptic Vesicle Pools

A number of potential mechanisms have properties that change their gain with activity, including ion channel inactivation, synaptic depression, and receptor desensitization. For AMPA-type glutamate receptors, desensitization and recovery are both rapid (<20 ms) (DeVries, 2000) and, thus, could not account for all parameters of the kinetics block. Kainate receptors do a have longer time constant of recovery (~1.5 s) but, again, could not account for the rate constants of slow inactivation and recovery in our model. Desensitization could, however, contribute a faster component of adaptation. An extension of the current model that accounted for desensitization would be to add a second kinetics block controlled by the output of the first.

We examined whether the kinetic parameters of the LNK model correspond to the properties of synaptic vesicle pools. Comparing the parameters of the bipolar-cell kinetics block to previously measured parameters of cone photoreceptor synaptic release under conditions that cause depression of photoreceptor synaptic release, replenishment of vesicles occurs with a time constant of ~250 ms (Rabl et al., 2006). This is substantially longer than the time constants of the bipolar-cell kinetics block, which were < 40 ms. In contrast to bipolar cell synaptic terminals, a large fraction of vesicles (~85%) in the photoreceptor terminal are available for release (Rea et al., 2004). Thus, under the stimulus conditions chosen here, vesicle depletion may not play a major role in bipolar cell contrast adaptation. A postsynaptic mechanism has been proposed for contrast adaptation in bipolar cells that require a change in intracellular calcium (Rieke, 2001). Although this mechanism is unknown, the kinetic parameters measured here serve as an important quantitative comparison for such candidate mechanisms.

However, we found a different result when comparing the kinetic properties of amacrine and ganglion cells to those of synaptic vesicle pools. Using the terminology of (Rizzoli and Betz, 2005), three pools include a RRP, a recycling pool, and a much larger reserve pool. We found that this framework can map directly onto the kinetics states of the LNK model. The resting state, $R$, corresponds to a state where sites in the recycling and RRP are filled. In the active state, $A$, fusion has occurred. The two inactivated states represent depletion of the two smaller pools. In the inactivated state, $I_1$, a site in the RRP is depleted, and in state $I_2$, a site in the recycling pool that refills the RRP is depleted. The activation rate constant $k_a$ corresponds to the rate of immediate release, and fast inactivation $k_{fi}$ corresponds to the rate of depletion of the RRP. The fast recovery rate constant $k_{fr}$ corresponds to the rate of refilling of the RRP from the recycling pool. Slow inactivation, $k_{si}$, represents the rate of depletion of the recycling pool, and slow recovery, $k_{sr}$, then represents the rate of recruitment from the reserve pool to the recycling pool.

To test whether the kinetics block parameters corresponded quantitatively to those of synaptic vesicle pools, we compared the parameters of the On pathway of nine amacrine and ganglion cells to those properties previously measured for On bipolar cell synaptic release. The rate of maximum release from the RRP depends on the membrane potential and, under physiological conditions, it is less than 120 $s^{-1}$. (Burrone and Lagnado, 2000). Our rate constant of activation ($k_a$) has a maximum value of 39 $s^{-1}$ ± 7. Using published measurements, this would be generated by a presynaptic depolarization of ~−32 mV within the expected physiological range of bipolar cells.

Two previously measured fast time constants of release differed by a ratio of 4–10, the slower of which is less than 0.5 s (Burrone and Lagnado, 2000). The three fast rate constants of our kinetics block will produce two fast time constants. By applying an impulse to the kinetics block, we found these to be 23.5 ± 4.1 ms and 197.6 ± 37.4 ms, differing by a ratio of 8.4 ± 0.8. The maximum rate constant of refilling of the RRP from the recycling pool has been measured to be 1.3 $s^{-1}$. Correspondingly, the rate constant of fast recovery, $k_{fr}$,was found to be 1.4 ± 1.8 $s^{-1}$, although in our case this rate was fixed and did not depend on the input. The maximum rate constant of refilling the recycling pool from the reserve pool has been found to be calcium-dependent and has been measured as 0.0013 (Gomis et al., 1999). Correspondingly, the rate constant of slow recovery, $k_{sr}$, was input-dependent, with a maximum of 0.0018 ± 0.0010 $s^{-1}$. To compare the rate of depletion of the recycling pool with our rate constant, $k_{si}$, we considered that the ratio of the depletion and refilling rates of the recycling pool (our $k_{si}$ and $k_{sr}$, respectively) will control the fractional occupancy of the reserve pool. The reserve pool has been estimated to hold 99.30% of vesicles (Neves and Lagnado, 1999), compared with 99.14% ± 0.25 estimated from the fractional occupancy of the kinetic states of the LNK model.

Although different rate constants of the LNK model can span a factor of > 10,000, they nonetheless correspond to previously measured values. Thus, starting directly from measured data of the membrane potential undergoing variance adaptation, the parameters of an accurate adaptive model match the known biophysical properties of synaptic release.

## DISCUSSION

We have shown that retinal contrast adaptation of the subthreshold potential corresponds closely to a model consisting of a nonadapting linear-nonlinear system followed by an adaptive first-order kinetics system. The LNK model accurately captures the membrane potential response, fast changes in kinetics, fast and slow changes in gain, fast and slow changes in offset, temporally asymmetric responses, and asymmetric time constants of adaptation. Because our goal was not only to

fit the response, but also to draw general conclusions about how adaptation can be implemented, we chose an adaptive component that has a strong correspondence to biophysical mechanisms. This allowed us to use the model to explain how each adaptive property can be produced by a single simple system.

Retinal ganglion cells were modeled using one or two parallel pathways, each with a single LNK stage. However, because bipolar, amacrine, and ganglion cells show adaptation, a more accurate circuit model would consist of two sequential LNK stages and parallel pathways to include amacrine transmission. Why does only a single LNK stage accurately capture ganglion-cell responses? Compared to the strong adaptation of ganglion cells, bipolar cell contrast adaptation to a uniform field stimulus is weak in the intact retina (Baccus and Meister, 2002), as opposed to when much of the inhibitory surround is removed in a slice preparation (Rieke, 2001). If this first adaptive stage is missing in a model, then the input to the second stage will have a greater change in variance across contrasts. However, this change in variance will be reduced by the stronger adaptation in the retinal ganglion cell stage, such that in the model, strong adaptation in the kinetics block will compensate for the absence of a weak initial adapting stage. Amacrine cells that have response properties that are similar to their target ganglion cells (Baccus et al., 2008) may be accounted for by a single-model pathway that represents the combined parallel effects of excitation and inhibition.

### Components of the LNK Model

In the model, the linear filter conveys an approximation of the stimulus feature encoded by the cell, and the nonlinearity conveys the strength of that feature. We chose the filtering stage to have a single stimulus dimension because it represents the more simple processing at the level of the photoreceptor or bipolar cell soma, as opposed to more complex features found in ganglion cells (Fairhall et al., 2006). The filter has a less direct correspondence to a biophysical mechanism, representing the combining effect of signal transduction and membrane and synaptic properties. For the nonlinearity, it is expected that the voltage dependence of calcium channels is a major contributor. These are, in fact, not instantaneous, although their kinetics are sub-millisecond (Mennerick and Matthews, 1996) and thus are effectively instantaneous at the timescale that we modeled. A more biophysical model would also translate this approximation into a kinetic model.

In the model, separate control over the internal mean and higher-order statistics allowed us to conclude that adaptation depends on the mean input to the kinetics block (Figure 6). We therefore predict that adaptation at the bipolar synaptic terminal depends only on the mean value of the internal calcium concentration. However, in an experiment, an attempt to separately control the mean and variance of the bipolar membrane potential or calcium concentration using visual stimuli would produce luminance adaptation, which can occur in as little as 0.1 s (Baylor and Hodgkin, 1974). A definitive experimental test of the prediction that the bipolar cell terminal adapts to the mean of the rectified membrane potential would bypass photoreceptors, directly manipulating the membrane potential or calcium concentration at the synaptic terminal.

Previous results indicate that adaptation to statistics beyond mean luminance is controlled primarily by standard deviation (Bonin et al., 2006). Our finding that contrast adaptation is controlled by the mean of an internal variable is not in conflict with this result. Because the initial filter combines multiple samples from the stimulus, due to the central limit theorem this will reduce the effects of higher-order moments of the stimulus, making the filtered stimulus more Gaussian. Thus, the standard deviation of the stimulus will have the largest control over the mean signal after it passes through the threshold nonlinearity. Because thresholds are common in the nervous system, it is likely that a signal with changing variance will be transformed to a signal with a changing mean, giving rise to the commonly observed properties of variance adaptation.

In the model, changes in the timescale of slow adaptation are produced by the variable rate constant of slow recovery, $k_{sr}$, which we found to be proportional to the contrast. Although our studies used a fixed time interval, this timescale of adaptation can change to match the timescale of changes in the stimulus contrast (Wark et al., 2009). Such plasticity of adaptive timescale would not automatically occur in our current model because such behavior would require $k_{sr}$ to depend on the timescale of contrast changes. If, as we propose, changes in $k_{sr}$ reflects the calcium dependence of slow vesicle mobility (Gomis et al., 1999), this would predict that this mechanism reflects an inference about the recent timescale of changes in stimulus contrast.

### Sites of Luminance and Contrast Adaptation

Our stimuli had a constant mean intensity and, thus, avoided luminance adaptation, which appears to be independent from contrast adaptation (Mante et al., 2005). Considering the source of this independence, we observed that the initial linear filter for amacrine and ganglion cells was strongly biphasic, transmitting little information about the mean luminance. Thus, one would expect that most luminance adaptation occurs at an earlier stage, whereas contrast adaptation would occur only after the threshold nonlinearity. However, at lower luminance the bipolar cell filter is more monophasic, transmitting more information about the mean luminance (Burkhardt et al., 2007). Accordingly, at low intensities, the bipolar cell terminal in the primate cone pathway does adapt to the mean luminance (Dunn et al., 2007). Because our results indicate that contrast adaptation is based on the mean signal at the bipolar cell terminal, adaptation to the mean luminance and contrast of the stimulus may not be independent at lower luminance.

### Modulation versus Intrinsic Adaptation

In principle, adaptive changes can be produced by one parallel pathway that modulates a second pathway (Mante et al., 2008; Cook and McReynolds, 1998). Parallel pathways have flexibility, in that stimuli that cause adaptation can differ from those encoded by the immediate response of the cell. This organization, however, requires additional neural circuitry to generate adaptation. In contrast, fast adaptive properties in the fly visual system have been captured by a more computational, multiple pathway model that adapts as an intrinsic aspect of motion detection (Borst et al., 2005).

Here, we find that all properties of retinal contrast adaptation are explained by a model with no such parallel pathway. Instead, transmission of the signal is naturally coupled to an intrinsic adaptation of the response, such that the process of transmitting a signal changes the rate of that transmission and depletes a store of that signal, leading to a change in temporal filtering, gain, and offset. Like adaptation to the mean luminance in the photoreceptor transduction cascade, contrast adaptation corresponds to a model of intrinsic adaptation.

### Relationship to Other Models

Other models of contrast adaptation have produced adaptive changes in sensitivity via a feedback pathway that subtracts a filtered version of the output signal (Gaudry and Reinagel, 2007; Victor, 1987). The LNK model differs in that the reduction of gain is produced not by a feedback inhibitory pathway, but rather by depleting a signal as it is transmitted. This architecture avoids the need for a feedback inhibitory pathway.

Integrate-and-fire (IF) type models qualitatively cause adaptive gain changes and small changes in temporal filtering (Gaudry and Reinagel, 2007; Keat et al., 2001; Pillow et al., 2005; Rudd and Brown, 1997). By comparison, the LNK model captures both neural responses and all adaptive properties across multiple contrasts, in particular full changes in kinetics and homeostatic fast and slow changes in response amplitude. For models of the IF type, each spike subtracts an afterpotential, causing refractoriness. However, large afterhyperpolarizations are not observed in retinal data following spiking (Kim and Rieke, 2001), and it is not clear how such a mechanism would cause adaptation measured in the subthreshold potential. Integrate-and-fire models can show similar behavior to kinetic models (Jolivet et al., 2004) and, thus, could provide a useful approximation for comparison to models with more direct biophysical significance.

The attraction of simple kinetic systems is that they are both amenable to analytic solutions and simulation and also have a correspondence with biophysical mechanisms. The adaptive properties of kinetic models that represent biochemical processes, including neurotransmitter receptors, have recently been analyzed from a theoretical point of view (Friedlander and Brenner, 2009). This previous work showed that first-order kinetic systems similar to the type discussed here can change their gain when receptors become unavailable. We extend these theoretical results to show how changes in temporal filtering and offset can also result from these simple systems. Other theoretical work has considered biochemical networks of two-state systems analogous to an enzyme with two different conformations, concluding that at least three such two-state systems are needed to produce adaptation (Ma et al., 2009). The system we have considered has fewer overall states but requires a signaling mechanism with at least three states. Our results highlight the greater adaptive power of molecules with at least three states, such as desensitizing receptors or inactivating ion channels.

### Toward Further Stages of Adaptation and Natural Vision

In a step toward understanding adaptation in natural scenes, full-field stimuli reduce the complexity of adaptive behavior, in that we could fit responses using one or two LNK pathways. More complex spatiotemporal stimuli will undoubtedly require additional pathways, such as adaptation to differential motion and spatiotemporal patterns (Hosoya et al., 2005; Olveczky et al., 2007). In a simple extension of these results, LNK pathways would represent different interneurons that adapt independently, consistent with one concept of how pattern adaptation could occur (Gollisch and Meister, 2010).

### Theoretical Explanations for Biophysical Properties

Variance adaptation embodies several theoretical principles of efficient coding. The change in gain allows a cell to use its dynamic range more efficiently (Laughlin, 1989). A change in temporal filtering and biphasic response helps to increase the integration time in an environment of weaker and, therefore, noisier signals (Atick, 1992; Van Hateren, 1993). Slow adaptation sets the timescale over which the statistics of the stimulus are measured (Wark et al., 2009). The temporal asymmetry between adaptation to low and high contrast corresponds to a statistical limitation in how fast the variance of a distribution can be measured (DeWeese and Zador, 1998). The LNK model shows how all of these adaptive principles can be implemented by microscopic transitions that are common to many biophysical mechanisms. Furthermore, the model establishes a correspondence between adaptation and depletion mechanisms that cause a signaling element to become temporarily inactivated upon its use. Because such depletion mechanisms are prevalent in the nervous system, this may reflect the widespread advantage for each signal to adapt to its own strength.

The parameters of the adaptive block of the LNK model bear great similarity to previously measured parameters of vesicle pools in the bipolar cell ribbon synapse. The correspondence of the LNK model to both adaptive computations and synaptic properties allows us to propose computational explanations for previously measured biophysical properties that have unknown functional benefits. The small number of vesicles in the RRP may be required so that release of few vesicles leads to a large change in gain. The rate constants of depletion and refilling of the RRP may be regulated differentially in different cells, so as to control adaptive changes in gain, kinetics, or temporal differentiation. Because we find that the inactivated state $I_1$ is needed to produce fast and slow subsystems with different adaptive effects, the presence of the recycling pool may be necessary so that the effects of fast and slow adaptation are distinct. The dominance of vesicles in the reserve pool may be a natural consequence of slow adaptation and necessary for the system to adapt over a sufficient timescale to measure the mean value of the synaptic input. The calcium dependence of the rate of recruitment from the reserve pool may reflect the statistical need to adapt over a longer time interval when the signal is weak. Thus, by making explicit the rules governing both the immediate light response and its adaptation over multiple time scales, we gain insight into how mechanisms can implement an adaptive neural code.

## EXPERIMENTAL PROCEDURES

### Electrophysiology

Intracellular recordings of 10–90 min were performed from the intact salamander retina as described (Baccus and Meister, 2002). Bipolar cells (n = 7),

adapting transient amacrine cells (n = 9), and ganglion cells (n = 7) were identified by their flash response, receptive field size, and level in the retina.

### Visual Stimulation

A spatially uniform visual stimulus lasting 300 s was projected from a video monitor. The stimulus intensity was drawn every 30 ms from a Gaussian distribution with mean intensity, $M$ (~8 mW/m$^2$), and standard deviation, $W$ (Smirnakis et al., 1997). Contrast was defined as $W/M$. Contrast changed every 20 s to a value between 0.05 and 0.35, drawn from a uniform distribution. The identical stimulus sequence was repeated at least two times.

### Linear Nonlinear Models

The linear temporal filter was computed by correlating the stimulus with the response as described (Baccus and Meister, 2002). The stimulus was convolved with the filter, yielding the linear prediction $g(t)$,

$$g(t) = \int F_{LN}(t-\tau)s(\tau)d\tau. \quad \text{(Equation 4)}$$

The filter was normalized in amplitude so that the variance of $g(t)$ and $s(t)$ were equal,

$$\int s^2(\tau)d\tau = \int g^2(\tau)d\tau. \quad \text{(Equation 5)}$$

Then, the fixed nonlinearity $N_{LN}(g)$ was calculated by averaging the values of $r(t)$ over bins of $g(t)$. The LN model output was calculated as

$$r'(t) = N_{LN}(g(t)) = N_{LN}\left(\int F_{LN}(t-\tau)s(\tau)d\tau\right). \quad \text{(Equation 6)}$$

Because of the normalization of the filter, $F_{LN}(t)$ summarizes temporal processing and $N(g)$ captures the sensitivity to the stimulus.

### Linear Nonlinear Kinetic Model

The stimulus, $s(t)$, was passed through a linear temporal filter, $F_{LNK}(t)$, and a static nonlinearity, $N_{LNK}(g)$,

$$u(t) = N_{LNK}\left(\int F_{LNK}(t-\tau)s(\tau)d\tau\right). \quad \text{(Equation 7)}$$

This is identical to an LN model, except that the filter and nonlinearity are different functions. The kinetics block of the model is a Markov process defined by

$$\frac{d\mathbf{P}^T(t)}{dt} = \mathbf{P}^T(t)\mathbf{Q}(u), \quad \text{(Equation 8)}$$

where $\mathbf{P}(t)$ is a column vector of $m$ fractional state occupancies, such that $\sum_i P_i = 1$ and $\mathbf{Q}$ is an $m \times m$ transition matrix containing the rate constants $Q_{ij}$ that control the transitions between states $i$ and $j$, with $Q_{ii} = -\sum_{i \neq j} Q_{ij}$. After this differential equation was solved numerically, the output of the model, $r'(t)$ was equal to one of the state occupancies scaled to a response in millivolts,

$$r'(t) = P_2(t)c + d, \quad \text{(Equation 9)}$$

where $c$ and $d$ are a scaling and offset term for the entire recording.

States and rate constants are defined as

| | | | | |
|---|---|---|---|---|
| $P_1 = R$ | Resting | $Q_{12} = u(t)k_a$ | Activation | (Equation 10) |
| $P_2 = A$ | Active | $Q_{23} = k_{fi}$ | Fast inactivation | |
| $P_3 = I_1$ | Inactivated | $Q_{31} = k_{fr}$ | Fast recovery | |
| $P_4 = I_2$ | Inactivated | $Q_{34} = k_{si}$ | Slow inactivation | |
| | | $Q_{43} = u(t)k_{sr}$ | Slow recovery. | |

The four state version of this model was

$$\frac{d\mathbf{P}^T(t)}{dt} = \begin{pmatrix} \dot{P}_1(t) \\ \dot{P}_2(t) \\ \dot{P}_3(t) \\ \dot{P}_4(t) \end{pmatrix} = \mathbf{P}^T(t) \begin{pmatrix} -u(t)k_a & u(t)k_a & 0 & 0 \\ 0 & -k_{fi} & k_{fi} & 0 \\ k_{fr} & 0 & -(k_{fr}+k_{si}) & k_{si} \\ 0 & 0 & u(t)k_{sr} & -u(t)k_{sr} \end{pmatrix}. \quad \text{(Equation 11)}$$

Some rate constants set to zero were initially allowed to vary in early fits but their optimal values were found to be near zero. Setting them to zero did not change the accuracy but did improve the speed of convergence of the model. For three-state models of bipolar cells, $P_4(t) = k_{si} = k_{sr} = 0$. Additional details about the fitting procedure can be found in Supplemental Experimental Procedures.

## SUPPLEMENTAL INFORMATION

Supplemental Information includes Supplemental Experimental Procedures and five figures and can be found with this article online at doi:10.1016/j.neuron.2011.12.029.

## ACKNOWLEDGMENTS

We thank D. Kastner and M. Manu for technical assistance. This work was supported by grants from the NEI, Pew Charitable Trusts, McKnight Endowment Fund for Neuroscience, the Karl Kirchgessner Foundation, the Alfred P. Sloan Foundation and the E. Matilda Ziegler Foundation (S.A.B.).

Accepted: December 20, 2011
Published: March 7, 2012

## REFERENCES

Atick, J.J. (1992). Could information theory provide an ecological theory of sensory processing? Network *3*, 213–251.

Baccus, S.A. (2006). From a whisper to a roar: adaptation to the mean and variance of naturalistic sounds. Neuron *51*, 682–684.

Baccus, S.A., and Meister, M. (2002). Fast and slow contrast adaptation in retinal circuitry. Neuron *36*, 909–919.

Baccus, S.A., Olveczky, B.P., Manu, M., and Meister, M. (2008). A retinal circuit that computes object motion. J. Neurosci. *28*, 6807–6817.

Baylor, D.A., and Hodgkin, A.L. (1974). Changes in time scale and sensitivity in turtle photoreceptors. J. Physiol. *242*, 729–758.

Beaudoin, D.L., Borghuis, B.G., and Demb, J.B. (2007). Cellular basis for contrast gain control over the receptive field center of mammalian retinal ganglion cells. J. Neurosci. *27*, 2636–2645.

Beaudoin, D.L., Manookin, M.B., and Demb, J.B. (2008). Distinct expressions of contrast gain control in parallel synaptic pathways converging on a retinal ganglion cell. J. Physiol. *586*, 5487–5502.

Bonin, V., Mante, V., and Carandini, M. (2006). The statistical computation underlying contrast gain control. J. Neurosci. *26*, 6346–6353.

Borst, A., Flanagin, V.L., and Sompolinsky, H. (2005). Adaptation without parameter change: Dynamic gain control in motion detection. Proc. Natl. Acad. Sci. USA *102*, 6172–6176.

Burkhardt, D.A., Fahey, P.K., and Sikora, M.A. (2007). Retinal bipolar cells: temporal filtering of signals from cone photoreceptors. Vis. Neurosci. *24*, 765–774.

Burrone, J., and Lagnado, L. (2000). Synaptic depression and the kinetics of exocytosis in retinal bipolar cells. J. Neurosci. *20*, 568–578.

Chander, D., and Chichilnisky, E.J. (2001). Adaptation to temporal contrast in primate and salamander retina. J. Neurosci. *21*, 9904–9916.

Chichilnisky, E.J. (2001). A simple white noise analysis of neuronal light responses. Network *12*, 199–213.

Colquhoun, D., and Hawkes, A.G. (1977). Relaxation and fluctuations of membrane currents that flow through drug-operated channels. Proc. R. Soc. Lond. B Biol. Sci. *199*, 231–262.

Cook, P.B., and McReynolds, J.S. (1998). Lateral inhibition in the inner retina is important for spatial tuning of ganglion cells. Nat. Neurosci. *1*, 714–719.

Demb, J.B. (2008). Functional circuitry of visual adaptation in the retina. J. Physiol. *586*, 4377–4384.

DeVries, S.H. (2000). Bipolar cells use kainate and AMPA receptors to filter visual information into separate channels. Neuron *28*, 847–856.

DeVries, S.H., and Schwartz, E.A. (1999). Kainate receptors mediate synaptic transmission between cones and 'Off' bipolar cells in a mammalian retina. Nature *397*, 157–160.

DeWeese, M., and Zador, A. (1998). Asymmetric dynamics in optimal variance adaptation. Neural Comput. *10*, 1179–1202.

Dunn, F.A., Lankheet, M.J., and Rieke, F. (2007). Light adaptation in cone vision involves switching between receptor and post-receptor sites. Nature *449*, 603–606.

Fairhall, A.L., Lewen, G.D., Bialek, W., and de Ruyter Van Steveninck, R.R. (2001). Efficiency and ambiguity in an adaptive neural code. Nature *412*, 787–792.

Fairhall, A.L., Burlingame, C.A., Narasimhan, R., Harris, R.A., Puchalla, J.L., and Berry, M.J., II. (2006). Selectivity for multiple stimulus features in retinal ganglion cells. J. Neurophysiol. *96*, 2724–2738.

Friedlander, T., and Brenner, N. (2009). Adaptive response by state-dependent inactivation. Proc. Natl. Acad. Sci. USA *106*, 22558–22563.

Gaudry, K.S., and Reinagel, P. (2007). Contrast adaptation in a nonadapting LGN model. J. Neurophysiol. *98*, 1287–1296.

Gollisch, T., and Meister, M. (2010). Eye smarter than scientists believed: neural computations in circuits of the retina. Neuron *65*, 150–164.

Gomis, A., Burrone, J., and Lagnado, L. (1999). Two actions of calcium regulate the supply of releasable vesicles at the ribbon synapse of retinal bipolar cells. J. Neurosci. *19*, 6309–6317.

He, Y., Zorumski, C.F., and Mennerick, S. (2002). Contribution of presynaptic Na(+) channel inactivation to paired-pulse synaptic depression in cultured hippocampal neurons. J. Neurophysiol. *87*, 925–936.

Heidelberger, R., and Matthews, G. (1992). Calcium influx and calcium current in single synaptic terminals of goldfish retinal bipolar neurons. J. Physiol. *447*, 235–256.

Hodgkin, A.L., and Huxley, A.F. (1952). A quantitative description of membrane current and its application to conduction and excitation in nerve. J. Physiol. *117*, 500–544.

Hosoya, T.H., Baccus, S.A., and Meister, M. (2005). Dynamic predictive coding by the retina. Nature *436*, 71–77.

Jolivet, R., Lewis, T.J., and Gerstner, W. (2004). Generalized integrate-and-fire models of neuronal activity approximate spike trains of a detailed model to a high degree of accuracy. J. Neurophysiol. *92*, 959–976.

Keat, J., Reinagel, P., Reid, R.C., and Meister, M. (2001). Predicting every spike: a model for the responses of visual neurons. Neuron *30*, 803–817.

Kim, K.J., and Rieke, F. (2001). Temporal contrast adaptation in the input and output signals of salamander retinal ganglion cells. J. Neurosci. *21*, 287–299.

Kim, K.J., and Rieke, F. (2003). Slow Na+ inactivation and variance adaptation in salamander retinal ganglion cells. J. Neurosci. *23*, 1506–1516.

Laughlin, S.B. (1989). The role of sensory adaptation in the retina. J. Exp. Biol. *146*, 39–62.

Luenberger, D.G. (1979). Introduction to Dynamic Systems: Theory, Models and Applications (New York: Wiley).

Ma, W., Trusina, A., El-Samad, H., Lim, W.A., and Tang, C. (2009). Defining network topologies that can achieve biochemical adaptation. Cell *138*, 760–773.

Manookin, M.B., and Demb, J.B. (2006). Presynaptic mechanism for slow contrast adaptation in mammalian retinal ganglion cells. Neuron *50*, 453–464.

Mante, V., Frazor, R.A., Bonin, V., Geisler, W.S., and Carandini, M. (2005). Independence of luminance and contrast in natural scenes and in the early visual system. Nat. Neurosci. *8*, 1690–1697.

Mante, V., Bonin, V., and Carandini, M. (2008). Functional mechanisms shaping lateral geniculate responses to artificial and natural stimuli. Neuron *58*, 625–638.

Mennerick, S., and Matthews, G. (1996). Ultrafast exocytosis elicited by calcium current in synaptic terminals of retinal bipolar neurons. Neuron *17*, 1241–1249.

Nagel, K.I., and Doupe, A.J. (2006). Temporal processing and adaptation in the songbird auditory forebrain. Neuron *51*, 845–859.

Neves, G., and Lagnado, L. (1999). The kinetics of exocytosis and endocytosis in the synaptic terminal of goldfish retinal bipolar cells. J. Physiol. *515*, 181–202.

Ohzawa, I., Sclar, G., and Freeman, R.D. (1985). Contrast gain control in the cat's visual system. J. Neurophysiol. *54*, 651–667.

Olveczky, B.P., Baccus, S.A., and Meister, M. (2007). Retinal adaptation to object motion. Neuron *56*, 689–700.

Pillow, J.W., Paninski, L., Uzzell, V.J., Simoncelli, E.P., and Chichilnisky, E.J. (2005). Prediction and decoding of retinal ganglion cell responses with a probabilistic spiking model. J. Neurosci. *25*, 11003–11013.

Rabl, K., Cadetti, L., and Thoreson, W.B. (2006). Paired-pulse depression at photoreceptor synapses. J. Neurosci. *26*, 2555–2563.

Rea, R., Li, J., Dharia, A., Levitan, E.S., Sterling, P., and Kramer, R.H. (2004). Streamlined synaptic vesicle cycle in cone photoreceptor terminals. Neuron *41*, 755–766.

Rieke, F. (2001). Temporal contrast adaptation in salamander bipolar cells. J. Neurosci. *21*, 9445–9454.

Rizzoli, S.O., and Betz, W.J. (2005). Synaptic vesicle pools. Nat. Rev. Neurosci. *6*, 57–69.

Rudd, M.E., and Brown, L.G. (1997). Noise adaptation in integrate-and fire neurons. Neural Comput. *9*, 1047–1069.

Shapley, R.M., and Victor, J.D. (1978). The effect of contrast on the transfer properties of cat retinal ganglion cells. J. Physiol. *285*, 275–298.

Shapley, R., and Victor, J.D. (1979). The contrast gain control of the cat retina. Vision Res. *19*, 431–434.

Smirnakis, S.M., Berry, M.J., Warland, D.K., Bialek, W., and Meister, M. (1997). Adaptation of retinal processing to image contrast and spatial scale. Nature *386*, 69–73.

Van Hateren, J.H. (1993). Spatiotemporal contrast sensitivity of early vision. Vision Res. *33*, 257–267.

Victor, J.D. (1987). The dynamics of the cat retinal X cell centre. J. Physiol. *386*, 219–246.

Wark, B., Fairhall, A., and Rieke, F. (2009). Timescales of inference in visual adaptation. Neuron *61*, 750–761.

Zaghloul, K.A., Boahen, K., and Demb, J.B. (2005). Contrast adaptation in subthreshold and spiking responses of mammalian Y-type retinal ganglion cells. J. Neurosci. *25*, 860–868.